Journal of the Korean Association for Shell and Spatial Structures
Vol. 4, No. 4 (통권 14호), pp. 99~111, December, 2004

Free Vibrations and Buckling of Rectangular Plates with Linearly Varying In-Plane Loading

장 경 호* 심 현 주** 강 재 훈***
Chang, Kyong-Ho Shim, Hyun-Ju Kang, Jae-Hoon

Abstract

An exact solution procedure is formulated for the free vibration and buckling analysis of rectangular plates having two opposite edges simply supported when these edges are subjected to linearly varying normal stresses. The other two edges may be clamped, simply supported or free, or they may be elastically supported. The transverse displacement (w) is assumed as sinusoidal in the direction of loading (x), and a power series is assumed in the lateral (y) direction (i.e., the method of Frobenius). Applying the boundary conditions yields the eigenvalue problem of finding the roots of a fourth order characteristic determinant. Care must be exercised to obtain adequate convergence for accurate vibration frequencies and buckling loads, as is demonstrated by two convergence tables. Some interesting and useful results for vibration frequencies and buckling loads, and their mode shapes, are presented for a variety of edge conditions and in-plane loadings, especially pure in-plane moments.

Keyword : Free Vibration; Buckling; Exact Solution; Rectangular Plates; Frobenius Method; Linearly Varying In-Plane Stresss.

1. INTRODUCTION

For more than a century researchers in structural mechanics throughout the world have endeavored to obtain accurate theoretical results for the free vibration frequencies and critical buckling loads of plates, as well as their corresponding mode shapes. Several thousands of research papers on these topics have appeared in the international scientific and technical journals and in conference proceedings, most of them dealing with rectangular plates. Much of the useful results has been summarized in monographs and handbooks.[1-6]

Rectangular plates subjected to uniform, static in-plane stresses have been extensively analyzed in both the vibrations and buckling literature. When the in-plane stresses vary throughout the plate the analysis is more formidable, and exact solutions for either type of problem are much more difficult to achieve. One finds considerable approximate results for plate buckling loads for such non-uniform stress fields, typically obtained by energy methods, but very little for the plate vibration problem.

The writers have recently looked into the case of the rectangular plate which has two opposite edges restrained by hinges or knife edges (i.e., "simply supported"), with these edges both having linearly varying normal stress (σ_x) acting on them (Fig. 1). This normal stress may be caused by a combination of longitudinal force and in-plane bending moment applied at each of the two simply supported edges. The other two

* 중앙대학교(서울) 건설환경공학과, 조교수
** 중앙대학교(서울) 건축학부, 박사과정
*** 정회원 · 중앙대학교(서울) 건축학부, 조교수

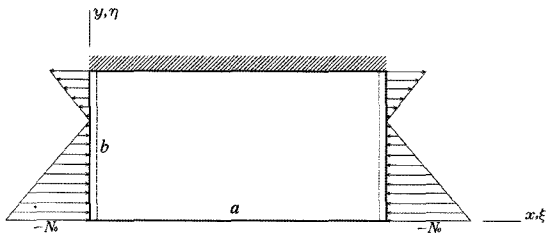

Fig. 1. An SS-F-SS-C rectangular plate loaded by linearly varying in-plane stresses.

edges may be clamped, simply supported or free. Although some buckling loads (but few mode shapes) obtained by energy methods are available in the published literature, the writers know of no free vibration results.

Exact solutions for the free vibration frequencies and buckling loads, and their mode shapes, may be obtained for the plates described above by using a power series representation for the transverse displacement (w) in the lateral (y) direction (i.e., the method of Frobenius). The writers have pursued this to obtain extensive results, which will be published in a series of research journal papers. In the present work, the method of analysis is shown, and some of the interesting results for frequencies, buckling loads and mode shapes are reported.

2. ANALYSIS

Consider a rectangular plate of lateral dimensions $a \times b$, as shown in Fig. 1, having its edges x=0 and x=a simply supported and linearly varying in-plane stresses at these two edges, whereas the other two edges (y=0 and y=b) may be either clamped, simply supported or free, and have no in-plane stresses. Assuming that the plate is thin, has uniform thickness, and that its material is homogeneous, isotropic and linearly elastic, the differential equation of motion governing vibration and buckling is[1)]

$$D\nabla^4 w + \rho h \frac{\partial^2 w}{\partial t^2} = q + N_x \frac{\partial^2 w}{\partial x^2} + 2N_{xy} \frac{\partial^2 w}{\partial x \partial y} + N_y \frac{\partial^2 w}{\partial y^2} \tag{1}$$

where w is transverse displacement; ρ is mass density per unit volume; h is the plate thickness; t is time; q is a distributed pressure per unit surface area applied to the lateral surface; ∇^4 is the bi-harmonic differential operator (i.e., $\partial^4/\partial x^4 + 2\partial^4/\partial x^2 \partial y^2 + \partial^4/\partial y^4$ in rectangular co-ordinates); D is the flexural rigidity of the plate defined by

$$D \equiv \frac{Eh^3}{12(1-\nu^2)} \tag{2}$$

E is Young's modulus; ν is Poisson's ratio; N_x and N_y are normal forces per unit length of plate in the x and y directions, respectively, positive if in tension; and N_{xy} is shearing force per unit length in the xy-plane. The forces (per unit length) are related to the in-plane stresses ($\sigma_x, \sigma_y, \tau_{xy}$) by $N_x = \sigma_x h$, $N_y = \sigma_y h$, and $N_{xy} = \tau_{xy} h$.

Let us assume $q = N_y = N_{xy} = 0$ and express N_x by the linear variation

$$N_x = -N_0 \left(1 - \alpha \frac{y}{b}\right) \tag{3}$$

where N_0 is the intensity of compressive force at the edge y=0 and α is a numerical factor. This stress distribution remains the same within the interior of the plate, and satisfies the plane elasticity equations exactly. By changing α, we can obtain various particular cases. For example, by taking $\alpha = 0$ we have the case of uniformly

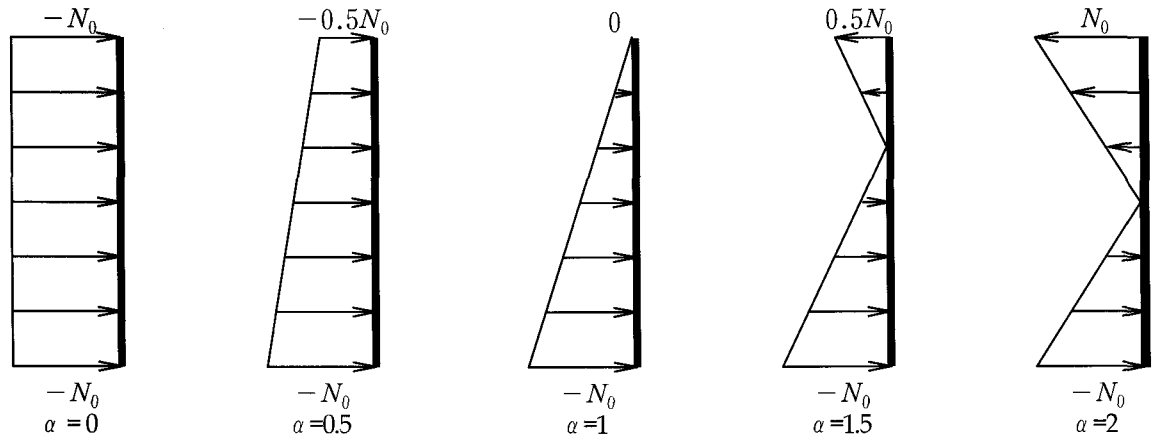

Fig. 2. Examples of in-plane loading N_x along the edge x=0.

distributed compressive force. When $\alpha=1$, the compressive force varies linearly from $-N_0$ at y=0 to zero at y=b. For $\alpha=2$ we obtain the case of pure in-plane bending. With other α in the range $0<\alpha<2$, we have a combination of bending and compression. Examples of these cases are shown in Fig. 2. For $\alpha<0$ or $\alpha>2$ the problems arising are identical with ones having $0<\alpha<2$ if the edge conditions at y=0 and b are considered properly. The governing equation of motion (1) reduces to

$$\nabla^4 w+\frac{\rho h}{D}\frac{\partial^2 w}{\partial t^2}+\frac{N_0}{D}\left(1-\alpha\frac{y}{b}\right)\frac{\partial^2 w}{\partial x^2}=0 \tag{4}$$

Adopting the non-dimensional coordinates $\xi\equiv x/a$ and $\eta\equiv y/b$, equation (4) becomes

$$\frac{\partial^4 w}{\partial\xi^4}+2k^2\frac{\partial^4 w}{\partial\xi^2\partial\eta^2}+k^4\frac{\partial^4 w}{\partial\eta^4}+\frac{a^4\rho h}{D}\frac{\partial^2 w}{\partial t^2}+\frac{a^2 N_0}{D}(1-\alpha\eta)\frac{\partial^2 w}{\partial\xi^2}=0 \tag{5}$$

where $k\equiv a/b$ is the aspect ratio.

A solution for the displacement w may be taken as:

$$w(\xi,\eta,t)=Y_m(\eta)\sin(m\pi\xi)\sin\omega t \tag{6}$$

where Y_m is a function of η, ω a natural frequency, and m the numbers of half-waves in mode shapes in the x direction. Equation (6) satisfies exactly the simply-supported boundary conditions at $\xi=0$ and 1. Substituting Eq. (6) into (5) yields

$$Y_m^{\mathrm{IV}}-2\beta_m^2 Y_m''+\left\{\beta_m^4-N^*(1-\alpha\eta)\beta_m^2-\frac{\lambda^2}{k^4}\right\}Y_m=0 \tag{7}$$

where Y_m^{IV} and Y_m'' are the fourth and second derivatives of Y_m with respect to η, respectively, β_m is defined by

$$\beta_m\equiv\frac{m\pi}{k}\quad(m=1,\ 2,\ 3,\cdots) \tag{8}$$

and λ and N^* are the nondimensional frequency and the compressive force at the edge y=0, respectively, defined by

$$\lambda\equiv\omega a^2\sqrt{\frac{\rho h}{D}} \tag{9}$$

$$N^*\equiv\frac{N_0 b^2}{D} \tag{10}$$

Equation (7) is an ordinary differential one in

η for each m. The ordinary differential equation has one variable coefficient in it, but it may be solved exactly by the method of Frobenius (i.e., a power series solution).

Let us assume the deflection function as

$$Y_m(\eta)=\sum_{n=0}^{\infty} C_{m,n}\,\eta^n \tag{11}$$

where $C_{m,n}$ is an arbitrary coefficient. Thus, we have derivatives as follows;

$$Y_m'(\eta)=\sum_{n=1}^{\infty} nC_{m,n}\,\eta^{n-1} \tag{12}$$

$$Y_m''(\eta)=\sum_{n=2}^{\infty} n(n-1)C_{m,n}\,\eta^{n-2} \tag{13}$$

$$Y_m'''(\eta)=\sum_{n=3}^{\infty} n(n-1)(n-2)C_{m,n}\,\eta^{n-3} \tag{14}$$

$$Y_m^{\mathrm{IV}}(\eta)=\sum_{n=4}^{\infty} n(n-1)(n-2)(n-3)C_{m,n}\,\eta^{n-4} \tag{15}$$

Substituting Eqs. (11), (13), and (15) into Eq. (7), we obtain

$$\begin{aligned}&\sum_{n=4}^{\infty} n(n-1)(n-2)(n-3)C_{m,n}\eta^{n-4}-2\beta_m{}^2\sum_{n=2}^{\infty}\\ &n(n-1)C_{m,n}\eta^{n-2}+\left(\beta_m{}^4-N^*\beta_m{}^2-\frac{\lambda^2}{k^4}\right)\sum_{n=0}^{\infty}\\ &C_{m,n}\eta^n+\alpha\beta_m{}^2N^*\sum_{n=0}^{\infty}C_{m,n}\eta^{n+1}=0\end{aligned} \tag{16}$$

Shifting indices, Eq. (16) becomes

$$\begin{aligned}&\sum_{n=0}^{\infty}\Big[\{(n+4)(n+3)(n+2)(n+1)C_{m,n+4}-2\beta_m{}^2(n+2)\\ &(n+1)C_{m,n+2}+\Gamma C_{m,n}\}\eta^n+\alpha\beta_m{}^2N^*C_{m,n}\eta^{n+1}\Big]=0\end{aligned} \tag{17}$$

where

$$\Gamma\equiv\beta_m{}^4-N^*\beta_m{}^2-\frac{\lambda^2}{k^4} \tag{18}$$

Using the property of identity, for the coefficient of η^0,

$$C_{m,4}=\frac{1}{6}\beta_m{}^2C_{m,2}-\frac{1}{24}\Gamma C_{m,0} \tag{19}$$

and for the coefficients of η^n $(n=1,2,3,\ldots)$

$$C_{m,n+4}=\frac{2\beta_m{}^2(n+2)(n+1)C_{m,n+2}-\Gamma C_{m,n}-\alpha\beta_m{}^2N^*C_{m,n-1}}{(n+4)(n+3)(n+2)(n+1)} \tag{20}$$

Equations (19) and (20) are the recursion relationships for $C_{m,n}$ when $n\geq 4$.

Thus, $C_{m,0}$, $C_{m,1}$, $C_{m,2}$, and $C_{m,3}$ are arbitrary coefficients, which will be used in two boundary conditions at each side ($\eta=0$ and 1), and the other coefficients $C_{m,n}$ for $n\geq 4$ are expressed in terms of them. Typically, the four boundary conditions yield four homogeneous equations with unknown $C_{m,0}$, $C_{m,1}$, $C_{m,2}$, and $C_{m,3}$. To obtain a non-trivial solution of the system, the determinant of the matrix of the coefficients is set to zero for the nondimensional frequencies (λ). One sees that the elements of the matrix have infinite series in them. Substituting each λ back into the four homogeneous equations yields the corresponding eigenvectors, $C_{m,n}/C_{m,0}$ (with n=1, 2, 3), which determines the mode shape.

There are three physically meaningful types of boundary conditions along the edges η=0 and η=1 for which this solution may be used[1]:

clamped: w=0 and $\dfrac{\partial w}{\partial y}=0 \;\Rightarrow\; Y_m=Y_m'=0$ (21a)

simply supported: w=0 and $M_y=0 \;\Rightarrow$

$$Y_m=Y_m''=0 \tag{21b}$$

free: $M_y = 0$ and $V_y = 0 \Rightarrow$

$$Y_m'' = Y_m''' + m^2\pi^2(2-\nu)Y_m' = 0 \qquad (21c)$$

Substituting Eq. (11) into one of the sets of boundary condition (21) for each of the two edges, η=0 and η=1, yields the fourth order characteristic determinant described earlier from which the eigenvalues (frequencies or buckling loads) may be found. In certain special cases, the determinant quickly reduces to a lower order one.

3. CONVERGENCE STUDIES

The exact solution functions given by Eq. (11) require summing an infinite series. Depending upon the degree of accuracy which one wants to have in numerical calculations, the upper limit of the summation is truncated at a finite number (N), which may be as large as needed. This procedure is no different than that followed in the evaluation of other transcendental functions arising in the exact solutions of other boundary value problems (e.g., Bessel functions, Hankel functions).

To examine the convergence rate of the power series of Eq. (11), the present equations are applied to the case of free vibrations of an SS-C-SS-C square plate under three loading conditions (α=0, 1, 2) for modes having two half-waves in the x-direction (m=2), when the load applied is on-half of the critical buckling value. This convergence study is shown in Table 1.

In Table 1 it is seen that for even the lowest frequency, which has a relatively simple mode shape with only one interior node line, at least 25 terms of the power series are required to obtain a reasonably accurate value of λ (37.36), whereas 31 terms are needed to obtain the frequency accurately to four significant figures (38.71). The

Table 1. Convergence of nondimensional frequencies $\lambda = \omega a^2\sqrt{\rho h/D}$ for an SS-C-SS-C plate with $a/b=1$, m=2, and $N_0/N_{cr}=0.5$

N	$\alpha=0$			$\alpha=1$			$\alpha=2$		
	1	2	3	1	2	3	1	2	3
25	37.36	2375	-	24.88	2396	-	2486	-	-
26	39.38	68.19	-	-	-	-	-	-	-
27	38.48	-	-	34.17	-	-	-	-	-
28	38.80	78.53	-	43.24	61.44	-	-	-	-
29	38.68	2081	-	37.89	2096	-	2161	-	-
30	38.72	84.08	-	39.72	76.48	-	-	-	-
31	**38.71**	87.56	115.9	38.89	-	-	25.97	-	-
32	38.71	85.90	-	39.22	83.66	-	-	-	-
33	38.71	86.46	132.0	39.09	88.67	118.8	38.27	2176	-
34	38.71	86.25	-	39.14	86.14	-	57.26	61.53	-
35	38.71	86.32	142.8	39.12	87.04	135.3	43.72	-	-
36	38.71	**86.30**	-	39.13	86.67	-	47.22	84.59	-
37	38.71	86.30	148.1	39.12	86.81	145.1	45.47	2284	-
38	38.71	86.30	150.7	39.13	86.76	154.3	46.20	92.99	-
39	38.71	86.30	149.6	39.12	86.78	149.0	45.88	98.81	134.1
40	38.71	86.30	150.0	**39.13**	**86.77**	150.6	46.01	95.82	-
41	38.71	86.30	149.8	39.13	86.77	149.9	45.96	96.96	148.1
42	38.71	86.30	**149.9**	39.13	86.77	150.2	45.98	96.47	162.6
43	38.71	86.30	149.9	39.13	86.77	**150.1**	**45.97**	96.67	153.7
44	38.71	86.30	149.9	39.13	86.77	150.1	45.97	96.59	156.4
45	38.71	86.30	149.9	39.13	86.77	150.1	45.97	96.62	155.2
46	38.71	86.30	149.9	39.13	86.77	150.1	45.97	**96.61**	155.6
47	38.71	86.30	149.9	39.13	86.77	150.1	45.97	96.61	**155.5**
48	38.71	86.30	149.9	39.13	86.77	150.1	45.97	96.61	155.5

underlined numbers in the table are those beyond which the fourth digit does not change as N increases. As more terms are taken the frequencies converge to their exact values. Data is not given in Table 1 for these modes for certain small numbers of terms because of the difficulty of the computer in establishing the roots of the frequency determinant in these cases.

Table 1 also shows that for the higher frequencies, having additional node lines in their corresponding mode shapes, more terms of the series are needed to represent the plate deformations properly. Thus, for example, for the third mode with α=2 (inplane moments), taking 42 terms or less yields a frequency which

Table 2. Convergence of nondimensional critical buckling moments $M_{cr}^{*} \equiv M/D$ of rectangular plates with two opposite edges simply-supported for $a/b=2.3$, $\alpha=2$, and $\nu=0.3$ by the power series method.

N	S-C-S-C (m=5)	S-C-S-S (m=5)	S-C-S-F (m=5)	S-S-S-C (m=4)	S-S-S-S (m=3)	S-S-S-F (m=3)	S-F-S-C (m=1)	S-F-S-S (m=1)	S-F-S-F (m=1)
5	-	-	-	-	-	-	1.615	.5771	.2498
7	16.02	-	-	-	6.543	-	3.017	1.312	.6253
9	3.764	-	-	38.27	7.025	26.95	3.352	1.660	1.067
11	1.204	-	-	-	53.58	-	3.779	1.903	1.424
13	.07537	-	-	51.81	34.94	36.03	3.908	1.983	1.583
15	.9309	.4502	-	-	3356	120.6	3.923	1.993	1.606
17	2.263	1.498	.6914	87.92	15.36	43.03	3.925	**1.994**	**1.610**
19	4.112	2.984	1.821	670.5	20.78	40.60	**3.925**	1.994	1.610
21	6.619	5.050	3.562	145.4	139.8	36.88	3.925	1.994	1.610
23	9.909	7.832	6.161	-	536.2	37.47	3.925	1.994	1.610
25	14.08	11.45	10.01	157.6	42.50	37.69	3.925	1.994	1.610
27	19.23	16.02	16.13	130.8	38.17	39.05	3.925	1.994	1.610
29	25.40	21.62	571.5	42.37	39.45	39.48	3.925	1.994	1.610
31	32.58	28.33	576.2	40.55	39.87	39.68	3.925	1.994	1.610
33	40.62	36.11	511.2	40.17	39.84	39.73	3.925	1.994	1.610
35	49.06	44.74	600.7	40.08	**39.83**	39.74	3.925	1.994	1.610
37	56.75	53.41	514.5	40.07	39.83	**39.75**	3.925	1.994	1.610
39	62.01	60.26	505.9	**40.06**	39.83	39.75	3.925	1.994	1.610
41	64.29	63.73	486.4	40.06	39.83	39.75	3.925	1.994	1.610
43	64.94	64.80	473.5	40.06	39.83	39.75	3.925	1.994	1.610
45	65.09	65.06	66.00	40.06	39.83	39.75	3.925	1.994	1.610
47	**65.12**	65.11	65.27	40.06	39.83	39.75	3.925	1.994	1.610
49	65.12	**65.12**	65.14	40.06	39.83	39.75	3.925	1.994	1.610
51	65.12	65.12	65.12	40.06	39.83	39.75	3.925	1.994	1.610
53	65.12	65.12	**65.11**	40.06	39.83	39.75	3.925	1.994	1.610
55	65.12	65.12	65.11	40.06	39.83	39.75	3.925	1.994	1.610

is highly inaccurate, but taking N=47 results in four-digit convergence (λ=155.5).

It is also interesting to note in Table 1 that the convergence is not monotonic. That is, the eigenvalues (λ) oscillate about the exact values as N is increased, rather than approaching them from one direction.

Buckling loads are obtained by setting $\lambda=0$ in the frequency determinants, thus establishing the load which reduces a natural frequency to zero. The lowest load thus determined is the critical buckling load.

Table 2 exhibits convergence studies for the critical buckling moments (i.e., $\alpha=2$) of plates with aspect ratio (a/b) of 2.3, for all nine possible, but distinct, combinations of the boundary conditions described by Eqs. (21). Thus, for example, the SS-F-SS-C plate (see Fig. 1) has a much lower critical moment (M/D=3.925) than that of the SS-C-SS-F plate (M/D=65.11). The SS edge conditions are abbreviated (to S) in Table 2. One also observes in Table 2 that the critical buckling mode shape of the SS-F-SS-C plate has only one half-wave in the loaded (x) direction (m=1), whereas the SS-C-SS-F plate has five. As before, it is seen that more terms of the power series are needed for four-digit convergence when more half-waves are in the mode shape.

4. SOME FREE VIBRATION RESULTS

One interesting configuration for which no free-vibration results have been previously published is the rectangular plate having three edges simply supported and one free, subjected to in-plane edge moments (i.e., α=2) at its opposite ends. Particularly interesting is the situation when the free edge is in tension, which is an SS-SS-SS-F plate in our notation.

Table 3 lists the first five nondimensional frequencies (λ) for three aspect ratios (a/b=0.5, 1, 2), with end moments M/M_{cr}=0, 0.5, 0.95 applied, where M_{cr} is the critical buckling moment for the plate. The results show that some of the frequencies decrease with increasing M, but others increase, and some first increase and then decrease. Thus, for some of the modes, the stabilizing effect of tension near the free edge (y=b) is more significant than the destabilizing effect of compression along the simply supported edge (y=0). This causes some of the frequencies to increase as M/M_{cr} is increased. But, eventually, the frequency for each mode decreases as the buckling moment for that mode is approached, and ultimately becomes zero with further increase in M. In following these trends in Table 3, one must consider a given mode, preserving one set of wave numbers (m, n), as M is changed.

Table 3. Nondimensional frequencies $\lambda \equiv \omega a^2\sqrt{\rho h/D}$ and critical buckling moments $M_{cr}^* \equiv M_{cr}/D$ for an SS-SS-SS-F plate (ν=0.3) subjected to end moments.

$\frac{M}{M_{cr}}$	mode sequence	a/b 0.5	1	2
0	1	10.30 (1,1)	11.68 (1,1)	16.13 (1,1)
	2	14.77 (1,2)	27.76 (1,2)	46.74 (2,1)
	3	23.62 (1,3)	41.20 (2,1)	75.28 (1,2)
	4	37.13 (1,4)	59.07 (2,2)	96.04 (3,1)
	5	39.77 (2,1)	61.86 (1,3)	111.0 (2,2)
0.5	1	10.26 (1,1)	17.06 (1,1)	42.28 (1,1)
	2	18.34 (1,2)	35.54 (1,2)	69.35 (2,1)
	3	24.66 (1,3)	41.04 (2,1)	83.31 (1,2)
	4	37.44 (1,4)	62.94 (1,3)	107.9 (3,1)
	5	38.89 (2,1)	73.36 (2,2)	139.6 (2,2)
0.95	1	3.468 (1,1)	8.265 (1,1)	37.05 (3,1)
	2	20.77 (1,2)	13.87 (2,1)	41.26 (2,1)
	3	26.84 (1,3)	43.54 (1,2)	44.43 (1,1)
	4	32.54 (2,1)	61.97 (3,1)	82.44 (4,1)
	5	37.97 (1,4)	64.85 (1,3)	95.40 (1,2)
M_{cr}/D		41.98 (1,1)	41.98 (2,1)	39.24 (3,1)

Note: The numbers in parentheses indicate (m,n) where m and n are the numbers of partial waves in the x and y directions, respectively, of a mode shape

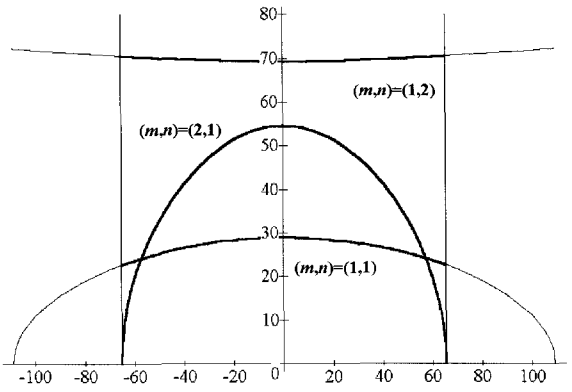

Fig. 3. Nondimensional frequencies $\lambda \equiv \omega a^2\sqrt{\rho h/D}$ vs. nondimensional moment $M^*(\equiv M/D)$ for an SS-C-SS-C plate with a/b=1 and α=2.

Similar trends are exhibited in Fig. 3 for the SS-C-SS-C square plate loaded by end moments. For no loading (M=0), the first three frequencies correspond to (1,1), (2,1) and (1,2) mode shapes, in that order. As M is applied, the first two frequencies decrease, the first one gradually and the second one rapidly, but the third frequency increases slightly. Eventually, as M is increased further, the (2,1) frequency curve crosses the (1,1) curve, and the plate buckles in a (2,1) mode. The (1,1) mode has a higher buckling moment. The (1,2) frequency decreases (beyond the abscissa limit of Fig. 3) and eventually goes

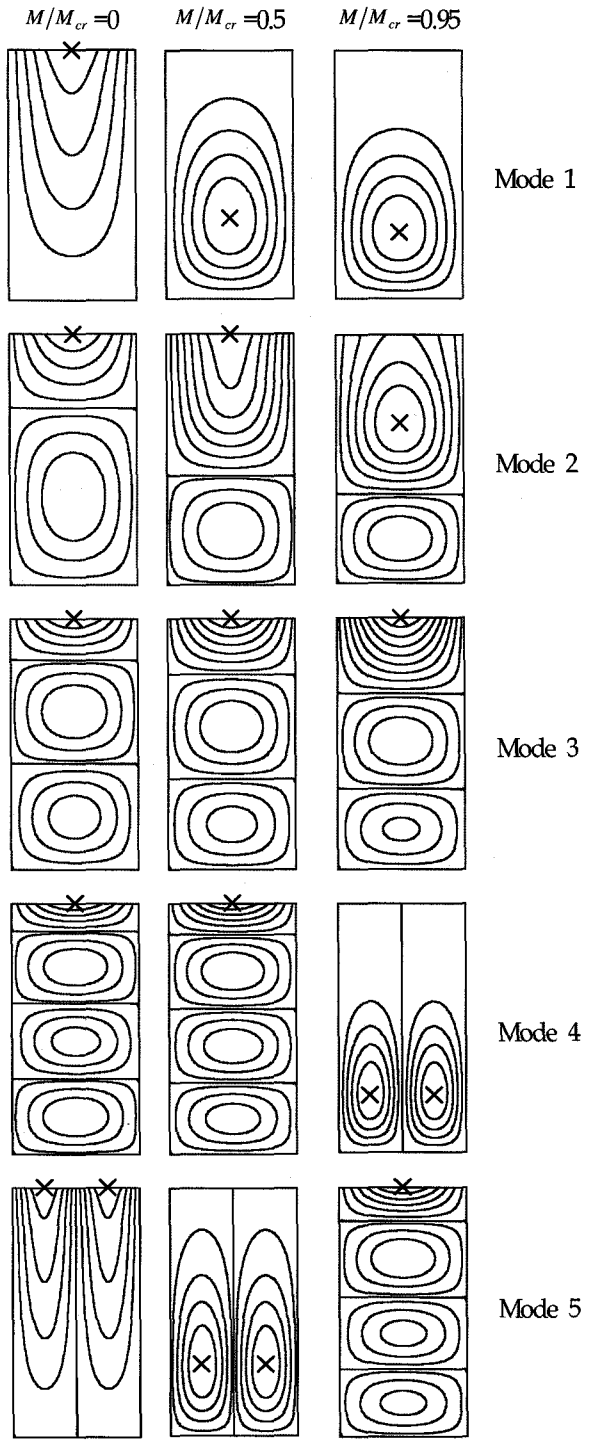

Fig. 4. Free vibration mode shape contour plots of SS-SS-SS-F plates with in-plane pure bending moments for a/b =0.5 and ν =0.3. (Maximum displacements marked with x.)

to zero at a large value of M/D.

Figures 4, 5 and 6 show contour plots of the free vibration mode shapes of SS-SS-SS-F plates

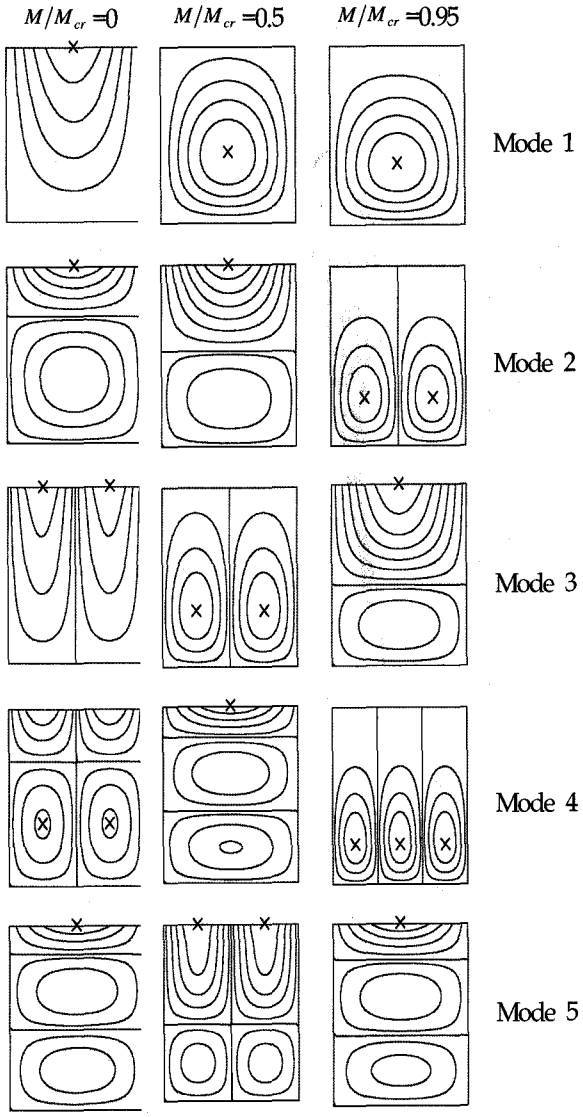

Fig. 5. Free vibration mode shape contour plots for SS-SS-SS-F plates with in-plane pure bending moments for a/b =1 and ν =0.3. (Maximum displacements marked with x.)

corresponding to the frequencies listed in Table 3. It is interesting to note how the contour lines shift downward (i.e., toward the simply supported, compressive lateral plate edge) as the end moment M is increased. This is true for all modes. For the (1,1) mode, which corresponds to the first frequency (except for a/b=2, M/M_{cr} =0.95), the point of maximum displacement moves from the free edge into the plate interior, and toward the SS lateral edge.

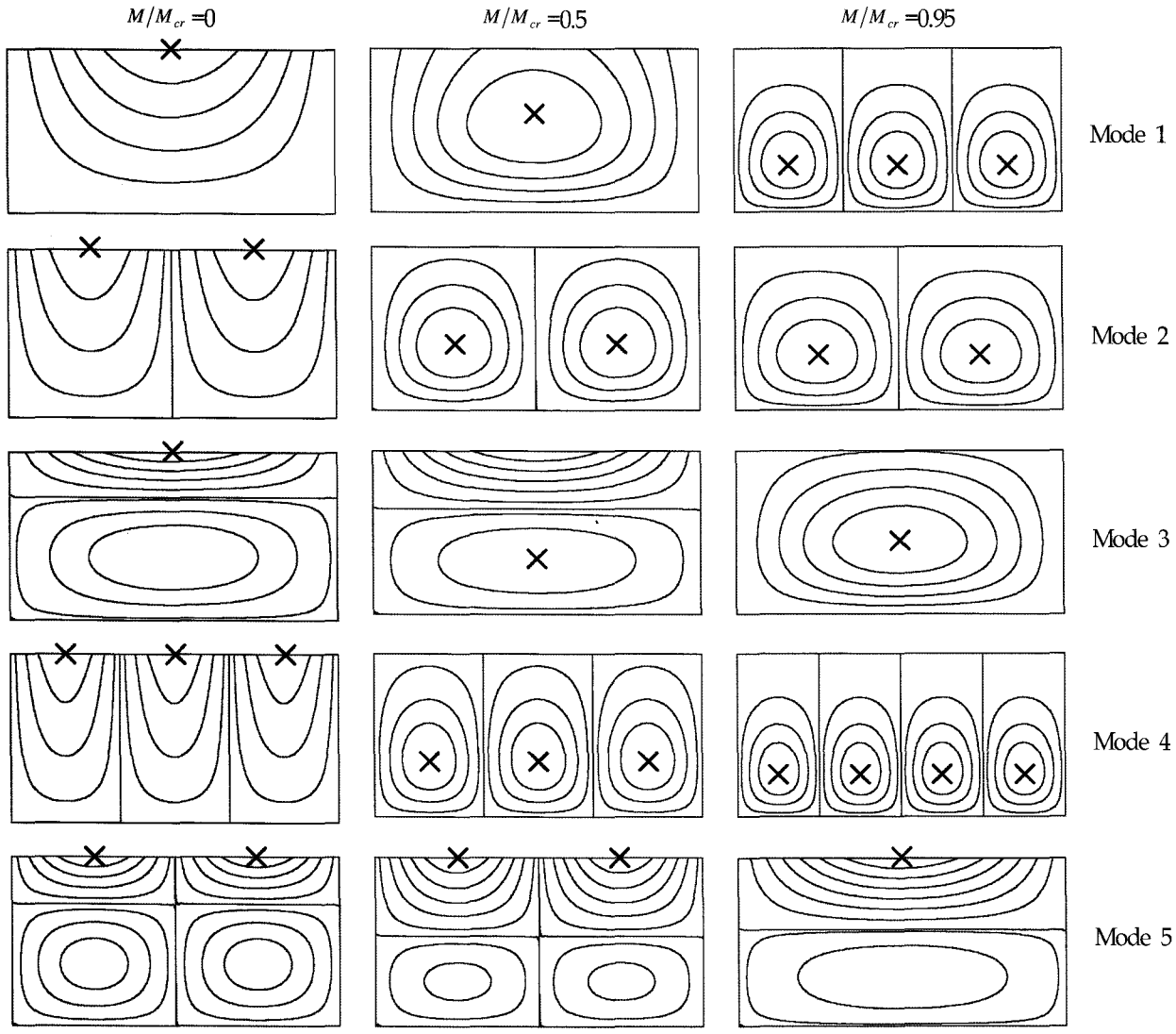

Fig. 6. Free vibration mode shape contour plots for SS-SS-SS-F plates with in-plane pure bending moments for a/b =2 and ν =0.3. (Maximum displacements marked with x.)

5. SOME BUCKLING RESULTS

It is interesting to observe how the critical buckling load varies as α changes. An example of this is shown in Fig. 7, where N_0b^2/D is plotted versus a/b for SS-C-SS-C plates. The case of uniform edge loading (α =0) is a classic one, for which a closed form solution for $w(x,y)$ exists, and is displayed in many places, including the classic monographs of Timoshenko and Gere[5] and Volmir.[6] This appears as the lowest envelope curve of Fig. 7, and shows the well known fact that the critical mode shape has an increasing number (m) of longitudinal half waves as the length-to-width ratio (a/b) increases. The critical modes all have only one partial wave in the y-direction.

Figure 7 also shows critical loads for the other linearly varying edge loadings exhibited in Fig. 2 (α =0.5, 1, 1.5, 2), obtained by the present power series method of analysis. As one increases α the buckling load parameter N_0b^2/D is seen to increase, as expected, because for a fixed N_0 the longitudinal force (i.e., the integral of σ_x over

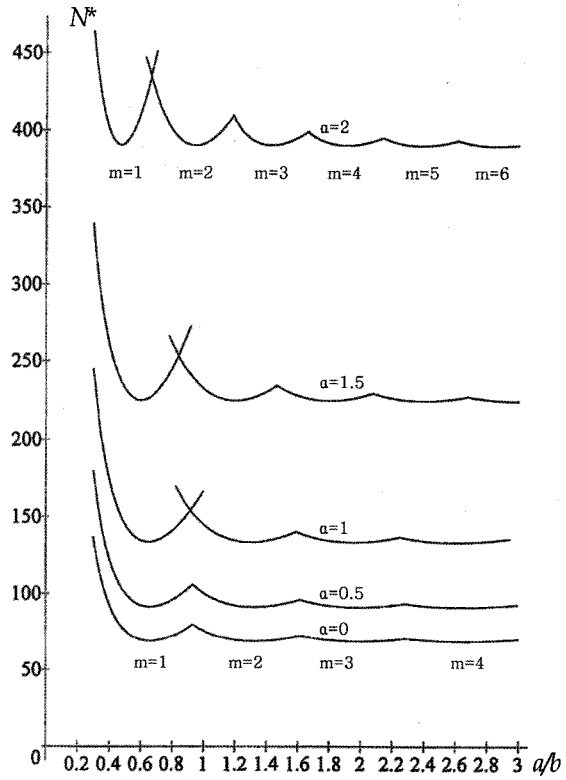

Fig. 7. Nondimensional critical buckling load $N^* \equiv N_0 b^2/D$ vs. aspect ratio a/b for SS-C-SS-C plates.

Table 4. Critical buckling loads $N^*_{cr} \equiv N_{cr} b^2/D$ for SS-F-SS-F plates.

a/b	ν	α				
		0	0.5	1	1.5	2
0.5	0	39.48	49.68	59.17	68.28	77.76
	0.3	38.42	47.62	55.26	62.43	69.78
	0.5	35.66	43.23	48.77	53.97	59.33
1	0	9.870	12.95	17.56	23.54	30.31
	0.3	9.399	12.27	16.21	20.79	25.73
	0.5	8.352	10.84	13.98	17.35	20.89
2	0	2.467	3.277	4.774	7.911	13.82
	0.3	2.292	3.040	4.389	6.990	11.26
	0.5	1.949	2.583	3.702	5.738	8.816
5	0	0.3948	0.5261	0.7853	1.508	5.365
	0.3	0.3608	0.4807	0.7165	1.360	4.296
	0.5	0.2992	0.3986	0.5935	1.118	3.309
10	0	0.09870	0.1316	0.1971	0.3900	2.670
	0.3	0.08991	0.1199	0.1795	0.3541	2.133
	0.5	0.07422	0.09894	0.1481	0.2916	1.638

the plate width) decreases. Not only do the curves shift upward with increasing α, but the number of longitudinal half-waves increases; for example, with a/b=2.8 the critical mode shape changes from m=4 for α=0, to m=6 for α=2.

The case of the SS-F-SS-F plate is a particularly important one. Table 4 displays critical buckling loads $N^*_{cr} \equiv N_{cr} b^2/D$ for such plates having various a/b (0.5, 1, 2, 5, 10), a variety of linearly varying loadings (α=0, 0.5, 1, 1.5, 2, as in Fig. 2), and the full range of possible Poisson's ratios for an isotropic material (ν=0, 0.3, 0.5). For α=0 (uniform loading) and ν=0, one observes that the critical buckling load is exactly that of an Euler column $\pi^2/(a/b)^2$; that is, for ν=0, there is no transverse (y) curvature in the mode shape. Nonzero ν induces transverse curvature (i.e., anticlastic bending). It would appear from Table 4 that increasing ν causes decreased N_{cr}, but that is not the case, for $D \equiv Eh^3/12(1-\nu^2)$ depends upon ν. A proper comparison of load parameters ($12N_{cr}b^2/Eh^3$) shows with a/b=1, for example, that N_{cr} increases by 12.8 percent as ν increases from 0 to 0.5.

Looking further at Table 4, for other α, N^*_{cr} increases with increasing α, as it did for the SS-C-SS-C plate in Fig. 7. Further, as α increases, the effect of ν becomes significantly different. For example, for a/b=1 and α=2 (in-plane moment) there is an 8.1 percent decrease in critical loading as ν increases from 0 to 0.5, as compared with the 12.8 per cent increase described above for α=0. It should also be mentioned here that all the critical mode shapes for the SS-C-SS-C plate have m=1, for all α, a/b and ν.

Contour plots (lines of constant displacement) of the critical buckling mode shapes for SS-F-SS-F plates are displayed in Fig. 8 for plates

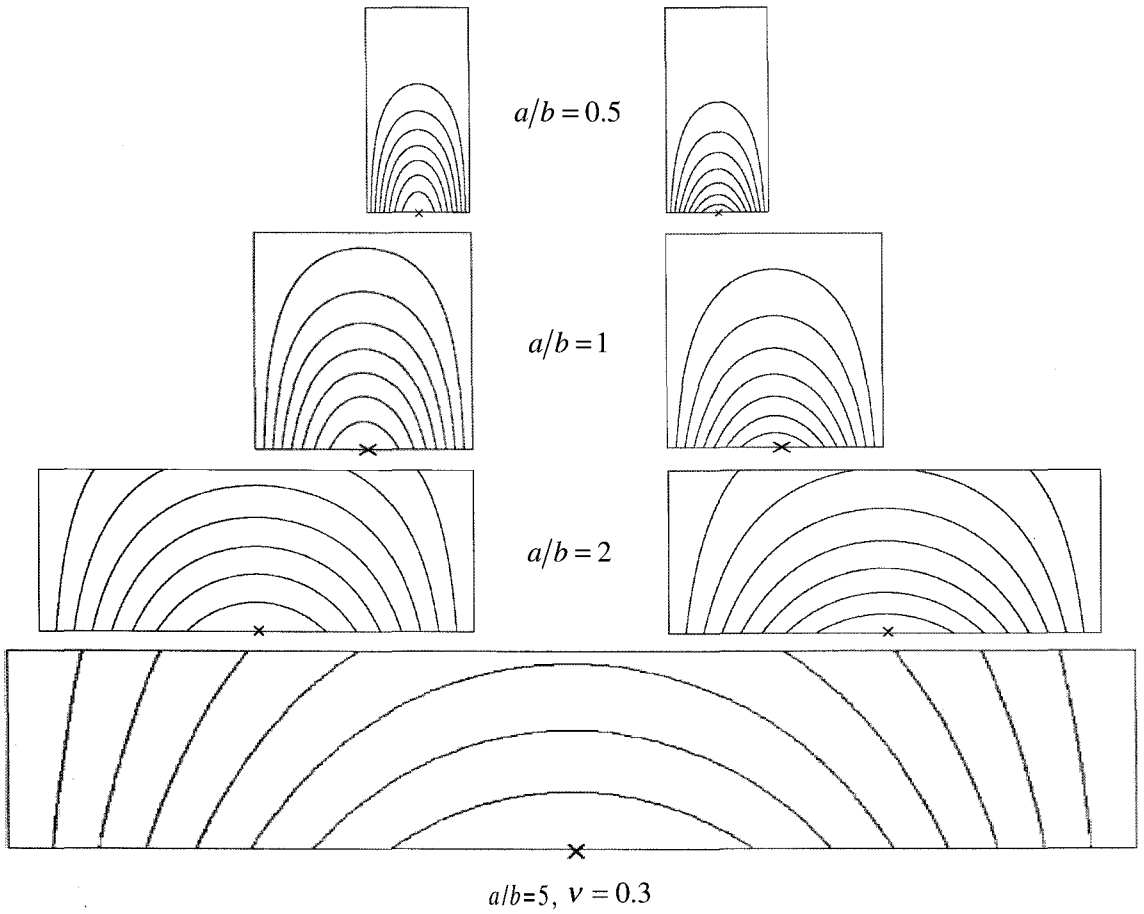

Fig. 8. Critical buckling mode shapes for SS-F-SS-F plates having various aspect ratios (a/b), loaded by in-plane moments (α =2) (points shown with × at a maximum displacement).

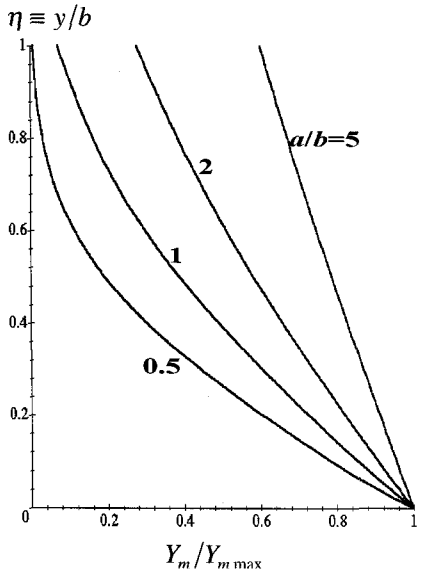

Fig. 9. Deflected shapes of the midlines ($x = a/2$) of the critical buckling mode shapes of SS-F-SS-F plates loaded by in-plane moments, for various a/b (for $\nu = 0.3$).

having a/b=0.5, 1, 2, and 5. In each case, the maximum transverse displacement in the mode shape occurs longitudinally in the middle (x=a/2) of the plate, and at the edge subjected to maximum compressive stress (y=0). For short plates (small a/b) the plate is seen to have anticlastic curvature (negative Gaussian curvature) in the mode shape throughout the plate, which is also observed in Fig. 9. For long plates (large a/b) the curvature in the lateral (y) direction virtually vanishes, as can be seen clearly in Fig. 9. Figure 8 also shows that an effect of increasing ν is to compact the contour lines more densely in the compressive zone, increasing the lateral curvature of the mode shape there.

The SS-F-SS-F plate may also be analyzed by

Table 5. Comparison of non-dimensional critical buckling moments M_{cr}/Eh^3 of SS-F-SS-F plates from 2-D plate theory using the power series method, and 1-D beam theory, for ν =0.3.

	a/b						
	0.5	1	2	5	10	20	50
1DB	.6495	.3247	.1624	0.06495	0.03247	0.01624	0.006495
2DP	1.065	.3928	.1718	0.06557	0.03255	0.01625	0.006495
Difference(%)	39.0%	17.3%	5.47%	0.946%	0.246%	0.062%	0%

one-dimensional (1-D) beam theory, as described by Timoshenko and Gere[5] in their Chapter 6 devoted to the sideways (called "lateral" there) instability of beams. Critical buckling end moments M_{cr}/Eh^3 from the beam theory are compared in Table 5 with those found from the more accurate plate theory using the present power series solution. It is seen there that (for ν =0.3) the beam theory is quite accurate for long plates, giving a critical moment within one percent of the plate result for $a/b>5$, and agreeing to four significant figures when a/b =50. However, one also sees that for short plates ($a/b<2$) the beam theory is inadequate. The beam theory does not permit the lateral curvature that one sees clearly in Fig. 9 for a/b <2, but assumes that the lateral lines remain straight, while rotating. The line shown in Fig. 9 for a/b=5 is almost straight.

6. CONCLUDING REMARKS

The exact solution procedure has been used to obtain a variety of interesting and useful results for frequencies, buckling loads and mode shapes of rectangular plates subjected to linearly varying in-plane stresses. Extensive results for the SS-F-SS-F plate having end moments only (α =2) are also available.[7]

The displacement functions (w) are expressed in terms of power series in the lateral (y) direction. As demonstrated by the results shown in Tables (1) and (2), extreme care must be taken to take enough terms in the series. Otherwise, very poor results may be obtained, even though as many as 30 terms are used. The power series are transcendental functions, similar to others commonly encountered in structural mechanics (e.g., trigonometric, hyperbolic, Bessel) which are also evaluated as power series, except that present ones have no "name" assigned to them.

Besides the clamped, simply supported or free edge conditions along the edges y = 0 and b (Fig. 1), these edges could also be restrained elastically (but uniformly) by adjacent support structure, in both transverse displacement and/or rotation, and the solution procedure would proceed straightforwardly. For the vibration problem, these edges could also have uniform attached mass and/or rotational inertia, perhaps also representing the support structure, with no restriction in the solution.

However, the in-plane boundary stresses cannot be generalized to others beyond that given by Eq. (3) for this exact solution method to apply. For more general boundary stresses, the plane elasticity problem would first have to be solved, which would yield in-plane stresses ($\sigma_x, \sigma_y, \tau_{xy}$) which would vary with both x and y. Then the variables separable solution form of Eq. (6) would no longer apply.

REFERENCES

1. Leissa, A.W., *Vibration of Plates*, U.S. Govt. Printing Office, Washington D.C., 1969, (reprinted by The Acoustical Society of America, 1993).
2. Leissa, A.W., "The free vibration of rectangular plates," J. Sound Vib., Vol. 31(3),

pp. 257-293, 1973.

3. Bulson, P.S., *The Stability of Flat Plates*, Chatto & Windus, London, 1970.
4. Japan Column Research Council, *Handbook of Structural Stability*, Corona Publishing Company, Tokyo, 1971.
5. Timoshenko, S.P. and Gere, J.M., *Theory of Elastic Stability*, 2nd Ed., McGraw-Hill, New York, 1963.
6. Volmir, A.S., *Stability of Deformable Systems* (in Russian), State Publishing House (Nauk), Moscow, 1967.
7. Kang, J.-H. and Leissa, A.W., "Vibration and buckling of SS-F-SS-F rectangular plates loaded by in-plane moments," Int. J. Struct. Stab. Dyn., Vol. 1(4), pp. 527-543, 2001.